Simulation of Millimetre-Wave Channels for Short-Range Body to Body Communications

Simon L. Cotton*, William G. Scanlon*, Bhopinder K. Madahar+

*Institute of Electronics, Communications & Information Technology
Queen's University Belfast, BT3 9DT, UK
{simon.cotton, w.scanlon}@qub.ac.uk

+Defence, Science & Technology Laboratory
Porton, SP4 0JQ, UK
bkmadahar@dstl.gov.uk

Abstract— **Operating short-range body centric communications at millimetre-wave frequencies will offer a number of key benefits, most notably high data rates potentially in excess of 2 Gb/s. However, development of compact, portable, bodyworn channel sounding equipment presents significant challenges at these frequencies. As an alternative method to characterising channel conditions for millimetre-wave applications, we present the steps taken to simulate body centric channels using animation software and a ray tracing algorithm. Using soldier-to-soldier communications as an example, a number of important channel metrics such as root mean square angle and delay spread are investigated.**

I. Introduction

Recent advancements in millimetre-wave (mm-wave) technology [1, 2] mean that it will soon be feasible to use operating frequencies in the 59-66 GHz range to provide high bandwidth capabilities for a range of body centric applications. The propagation characteristics at this part of the spectrum will provide many benefits for short-range body centric communications, especially in densely populated areas. For example, the higher path loss, when compared to lower microwave bands, will lead to a reduction in inter-body area network (BAN) interference between co-located BAN users. Body-to-body networks (BBNs), where signal propagation occurs from wearable wireless devices situated on one person to other nearby persons will benefit from better frequency reuse due to much shorter hops. Furthermore, the combination of high densities of people and mm-wave networking could be leveraged to provide cooperative communications, whereby active users designate a proportion of their bandwidth for usage by others. The short signal wavelength ($\lambda \approx 5$ mm), will also support the development of truly miniaturised devices.

Driven by the development of commercial networking standards, e.g., IEEE 802.15.3c and IEEE 802.11ad, innovations in mm-wave communications will be of particular interest to the military, especially in urban warfare environments. Here, the range of electronic equipment available to future infantry soldiers will see dramatic improvements with the introduction of high-resolution digital video cameras, helmet mounted displays and body sensor networks that will operate alongside established technologies such as voice communications and navigational aids. The bandwidth necessary for synchronous multichannel streaming coupled with the diversity of future battlefield operations will increase the demand for high-speed wireless networking between dismounted combat personnel. In this paper, we describe the steps taken to simulate signal propagation in this important application of body-to-body networking.

II. Simulation of MM-Wave Body Centric Channels

A range of electromagnetic solver tools are available for simulating signal propagation in wireless channels. Of these, the finite-difference time-domain (FDTD) and ray tracing methods are of particular interest. FDTD modelling works by solving Maxwell's equations in the time domain. The FDTD method becomes computationally intractable over large distances at mm-wave frequencies due to high number of Yee cells required to achieve an accurate result [3]. Another approach, which is based upon geometrical optics (GO) and the uniform theory of diffraction (UTD), is ray tracing (RT). In ray launching implementations of RT, the transmit antenna launches N rays over a selected spatial angle. The algorithm then tracks each of the rays until it illuminates the area of interest or until the power of the ray falls below a preselected threshold level. Because the method is based upon GO, as the frequency of the carrier increases, the approximation of ray launching to signal propagation improves. A particular strength of using RT simulation methods to make channel predictions is that they allow infinite resolution of transmitted and received signal contributions in both time and space.

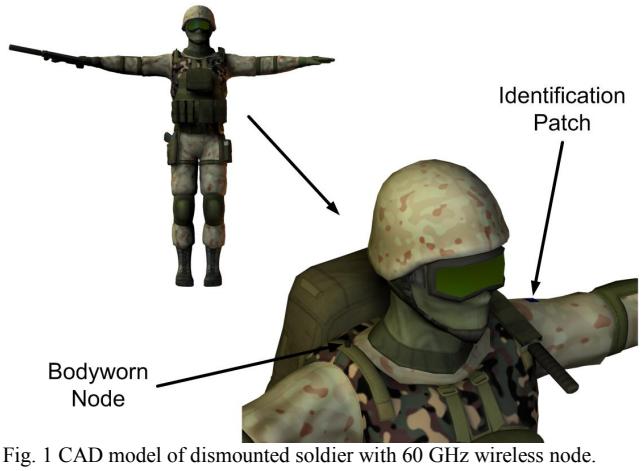

Fig. 1 CAD model of dismounted soldier with 60 GHz wireless node.

This feature makes them inherently suitable for generating transmission channel information to be used in conjunction with network simulators (e.g., OPNET, NS2 etc.), allowing time/direction of arrival based protocols to be rigorously tested. To illustrate the use of ray launching in the simulation of signal propagation in BBNs, we now describe the simulation of the mm-wave channel between a team of four dismounted combat personnel performing a hypothetical counter-insurgency cordon and sweep operation.

A particular problem with achieving realistic transmission channel predictions in scenarios that involve the human body is the encapsulation of movement. One possible solution to this problem is the use of animation software to generate the required dynamics. These programs typically allow the straightforward manipulation of user-created, 3-D polymesh human figures with the ability to export the animation sequence to a native file format readily interpreted by computer aided design (CAD) software (e.g., drawing exchange format). Fig. 1 shows an example of the soldier model (height 1.83 m) used in this study generated using the Poser 7 animation software[1]. The lifelike model of the US infantry soldier includes the improved outer tactical vest and lightweight helmet, backpack, pouches and weaponry. Also shown in Fig. 1 is a single 60-GHz wireless node positioned on the right shoulder which, for simulation purposes, was fitted with a vertically polarized (when soldier is standing upright) dipole antenna, chosen because of its favourable omnidirectional radiation characteristics in the azimuth. The computer generated environmental model created for this study was designed using the AutoCAD software package. It was based upon a small compound as encountered by coalition troops in the Middle East as shown in [Fig. 3, 4].

III. Body-to-Body Simulations

The simulations followed three distinct stages of a cordon and sweep type operation, and modelled bidirectional signal propagation between a squad of four US infantry troops. The dynamic transmission channel simulations used a full 3-D RT (ray-launching) algorithm [5] that was set to calculate all reflections, penetrations and diffractions. A library of purposely written executables were responsible for the amalgamation of the animation sequence and CAD environment model, assignment of dielectric properties to material layers, transmit power and other related channel simulation properties as well as controlling the automation of the ray launching algorithm. Proprietary software also tracked the changes in antenna orientation (i.e., pattern rotation) caused by soldier movements in 3-D vector space. The soldiers were given movements and speeds relative to their role within the operation. The animations were performed at a rate of 50 frames per second, which for the purposes of ray launching simulation is analogous to 50 samples of the mm-wave channel per second. The 60-GHz wireless nodes were set to transmit at a power level of +20 dBm.

[1] http://www.smithmicro.com/poser/

The overall simulation scenario was designed to encompass a wide range of channel types: indoor, outdoor and indoor to outdoor. Stage 1 involved movement of the team from a "drop-off zone" beside the Abrams M1 tank [Fig. 3, 4], to the entrance of an enemy command centre and analysed outdoor body-to-body signal propagation (Fig. 2). This stage took approximately 5 s to complete. Stage 2, duration 4.5 s, investigated both indoor and outdoor-to-indoor signal propagation as three of the team swept the building, while the remaining soldier maintained guard at the entrance (Fig. 3). Finally, Stage 3 (Fig. 4), lasted for 5.2 s and studied the movement of the team within a large multi-room structure.

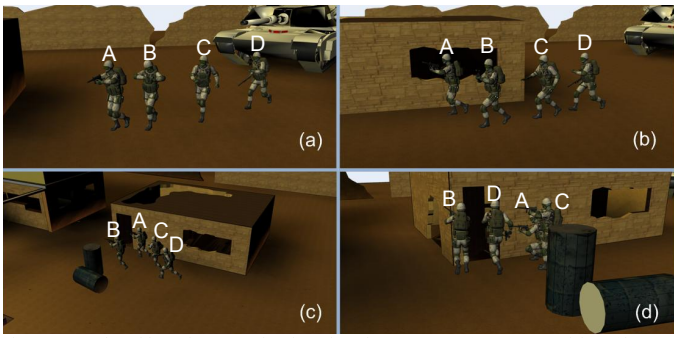

Fig. 2 Sample of key frames of animation for Stage 1: (a) start position (frame 1), (b) crossing front of building, (c) approaching doorway, (d) end position.

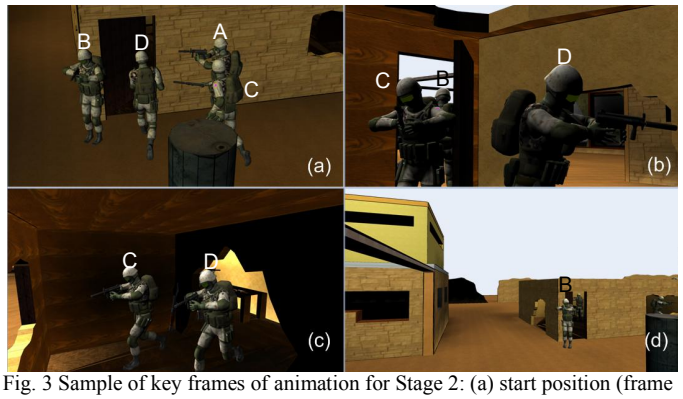

Fig. 3 Sample of key frames of animation for Stage 2: (a) start position (frame 1), (b) soldiers C and D entering building, (c) soldier C and D clearing front room, and (d) end position.

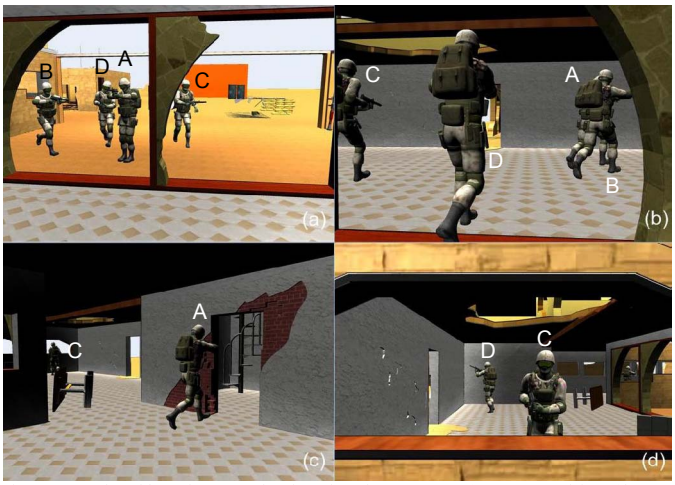

Fig. 4 Sample of key frames of animation for Stage 3: (a) start position (frame 1), (b) soldiers entering main foyer of building, (c) soldier A moving into back room, (d) end position.

IV. RESULTS

In this section, we present a selection of the results obtained from the simulations described above to demonstrate typical mm-wave channel characteristics for body-to-body communications. Angle of arrival (AOA) statistics such as the root mean square (rms) angle spread are presented alongside important wideband channel parameters such as power delay profiles and rms delay spread. The latter two can be used to investigate the potential impact of intersymbol interference (ISI) and its ramifications for wideband receiver design.

A. Angle of Arrival

Smart antenna technology, which is able to apply signal gain in carefully chosen directions, can be used to overcome signal shadowing and blocking and will undoubtedly become a key feature of emerging mm-wave wireless systems. The successful implementation of these technologies for use in future BBN applications will be highly dependent upon a thorough knowledge of channel characteristics relative to deployment. The azimuth (or elevation) rms angle spread of the channel impulse response is a measure of the angular dispersiveness of the channel [6]. A transmission channel in which major signal components arrive from significantly different spatial orientations is characterized by a large rms angle spread and vice versa. The azimuth (or elevation) mean angle may be defined as the first central moment of the azimuth (or elevation) spectrum given by [7]:

$$\bar{\theta} = \frac{\sum_{i=1}^{N} P(\theta_i)\theta_i}{\sum_{i=1}^{N} P(\theta_i)} \quad (1)$$

where θ_i and $P(\theta_i)$ are the AOA and power of the i^{th} component respectively. Following from this, the azimuth (or elevation) rms angle spread, σ_θ, is defined as the second central moment of the azimuth (or elevation) spectrum as follows [7]:

$$\sigma_\theta = \sqrt{\overline{\theta^2} - (\bar{\theta})^2} \quad (2)$$

where

$$\overline{\theta^2} = \frac{\sum_{i=1}^{N} P(\theta_i)\theta_i^2}{\sum_{i=1}^{N} P(\theta_i)} \quad (3)$$

The azimuth and elevation rms angle spreads were calculated at each simulation time step (animation frame) for individual soldier-to-soldier links. Fig. 5 summarises these results by presenting the cumulative distribution functions (CDFs) of rms angle spread over all the simulations (all three stages) and for all bidirectional links. For stage 1, the azimuth rms angle spread had a 90 percent probability of being less than 90°. The corresponding figure for the elevation rms angle spread was lower at 20°, an observation most likely to have been caused by the fact that each of the soldiers were of the same height and were vertically upright for the duration of stage 1. These results provide solid evidence of the directional characteristics of the outdoor mm-wave body-to-body transmission channel. This will be attractive to military systems designers wishing to provide a good degree of covertness (low probability of *detection* or *interception*).

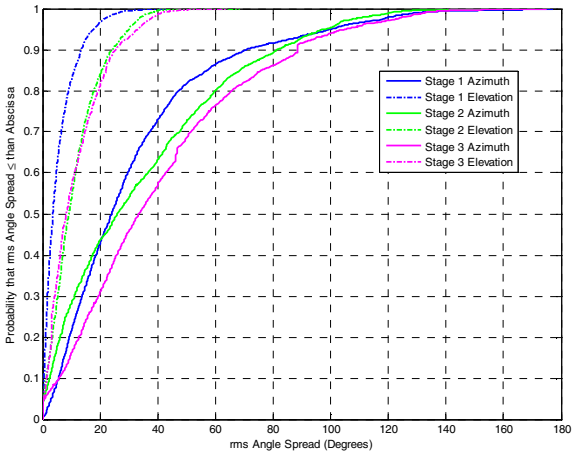

Fig. 5 CDFs of rms angle spread over the three stages of simulation for all bidirectional links [Fig 4, 4].

For stage 2, rms angle spread for both azimuth and elevation planes were increased compared to stage 1 (Fig. 5). The increase in rms angle spread, especially elevation, within indoor environments was to be expected, and may be explained by the larger number of multipath components caused by the close proximity of scattering and reflecting objects such as walls, ceilings, and furniture. In stage 3 of the operation, the rms angle spread also increased compared to stage 1. The results from stages 2 and 3 show quite clearly that rms angle spread increases as the soldiers move from a mostly uncluttered LOS outdoor communications scenario to an often obstructed indoor communications one. Furthermore, the rich multipath conditions observed within indoor environments at 60 GHz should generate enough signal components with sufficient angular separation to sustain short-range soldier-to-soldier communications should the main signal path become unexpectedly shadowed or blocked.

B. Time of Arrival

The amplitude and propagation delays of the multipath components transmitted between mobile dismounted combat personnel can be modelled as a linear time-variant filter. The impulse response of this channel $h(t,\tau)$ is a function of the time, t, and the delay τ and may be defined as [8]:

$$y(t) = \int_{-\infty}^{\infty} x(t-\tau)h(t,\tau)d\tau \quad (4)$$

where $x(\cdot)$ is the transmitted signal and $y(t)$ is the received signal. If the channel changes at a much slower rate than the duration of the impulse response, then the behaviour at a time t is like a linear time-invariant filter with corresponding channel impulse response $h(\tau)$, and the system is said to be quasi-static. Due to the complexity of developing and analysing the autocorrelation function of time-variant channels, another simplification that is also applied is the assumption of Wide Sense Stationary Uncorrelated Scattering (WSSUS) [8]. For a process to be considered wide sense stationary (WSS), the mean value of the process must be independent of time and its autocorrelation function must not depend upon the two time instants t_1 and t_2, but rather their time separation, Δt, i.e. $\Delta t = t_2 - t_1$. Furthermore, if

uncorrelated scatterers (US) are assumed, the phase of an incoming multipath component does not contain any information about the phase of other signal contributions arriving via different propagation paths.

When a system has infinitely wide bandwidth, the WSSUS channel can be represented as a tapped delay line with the following discrete time impulse response [6]:

$$h(t,\tau) = \sum_{i=1}^{N(t)} a_i(t) * \exp\big(j\varphi(t)\big) * \delta\big(\tau - \tau_i(t)\big) \quad (5)$$

where $N(t)$ is the (time-variant) number of multipath components, $a_i(t)$, $\varphi(t)$ and $\tau_i(t)$ are the time-variant amplitude, phase and time of arrival of the i-th multipath component, respectively and $\delta(\cdot)$ denotes the delta function. A more typical method of presenting the amount of energy which arrives at a receiver with a time delay that falls in the interval $[\tau, \tau + d\tau]$ is the power delay profile (PDP), $P(\tau)$, obtained from the complex impulse response as [8]:

$$P(\tau) = \int_{-\infty}^{\infty} |h(t,\tau)|^2 d\tau \quad (6)$$

Based upon the discrete-time impulse response model presented in (5), the discrete-time PDP can be expressed as [7]:

$$P(\tau) = |h(t,\tau)|^2 = \sum_{i=1}^{N(t)} \beta_i^2 * \delta\big(\tau - \tau_i(t)\big) \quad (7)$$

where β_i is the amplitude of the i^{th} multipath component. From the PDP a number of important statistics may be extracted which describe multipath behaviour of the wideband channel. These include the rms delay spread, which under certain conditions, has been shown to be proportional to the error probability due to delay dispersion [7]. In these specific cases, rms delay spread fully characterizes the channel. The rms delay spread, σ_τ, may be defined as the square root of the second (order) central moment (or centred) moment of the power delay profile and is defined for the discrete-time PDP as [7]:

$$\sigma_\tau = \sqrt{\overline{\tau^2} - (\bar{\tau})^2} \quad (8)$$

where the mean excess delay is given by the power weighted average (β_i^2) of the excess delays (τ_i):

$$\bar{\tau} = \frac{\sum_{i=1}^{N} \tau_i \beta_i^2}{\sum_{i=1}^{N} \beta_i^2} \quad (9a)$$

$$\overline{\tau^2} = \frac{\sum_{i=1}^{N} \tau_i^2 \beta_i^2}{\sum_{i=1}^{N} \beta_i^2} \quad (9b)$$

It should be noted that in reality, the WSSUS assumptions used to derive the equations (4) to (9) must hold for any arbitrary time *t*. In practice, this will not be possible for body-to-body links as either end of the link moves over larger distances and the mean power level will change due to shadowing and variations in path loss. One advantage of using an RT simulator to make body-to-body channel predictions is that all signal contributions can be fully resolved both in time and space, something which is not possible in practical systems. Due to the infinite resolution available in the RT simulation, we make the assumption that the channel is stationary over the duration of the acquisition of the channel impulse response. Therefore, in this paper, we analyse the statistical dispersion of the rms delay spread over the duration of the entire simulation.

When high data rate systems operate under dispersive channel conditions, they can be subject to ISI which can significantly degrade the performance of wireless networks. The rms delay spread is considered as the most important single parameter for defining the time-extent of a time-dispersive radio channel [9]. Fig. 6 shows the power delay profiles (PDPs) for the wireless link from soldier B to soldier A. It can be seen quite clearly that the vast majority of the energy is contained within the direct path which typically arrives within 25 ns. Fig. 6 also shows the existence of occasionally significant multipath components which arrive between 100 and 150 ns. For practical mm-wave wireless systems operating in an outdoor environment, multipath signal contributions arriving at the receiver due to interactions with distant objects will experience higher path loss compared to systems that function at lower frequencies. This will mean that the rms delay spreads observed in outdoor mm-wave wireless channels can be expected to be lower than those operating at lower frequencies. A summary of the rms delay spread statistics for all bidirectional soldier-to-soldier links for stage 1 are provided in Table 1.

In stage 2, the rms delay spread ranged from ≈0 ns for the links between soldiers A & D and B & D to 96.11 ns for the link between soldiers B & C as shown in Table 2. The median rms delay spread was typically low, falling in the range 3.53 to 8.94 ns. The IQR rms spread was much lower than stage 1 due to much shorter contributing path lengths. For the link between soldiers A and B, the bulk of which forms an indoor to outdoor link, the shape of PDPs given in Fig. 7 shows that the vast majority of the signal energy is made up of very few multipath components, and arrives with very little delay. Another interesting observation, which can be made from Fig. 7, is the increasing delay in time of arrival and decrease in power level for the main signal components and the rapid deterioration of the link towards the end of this stage of operations.

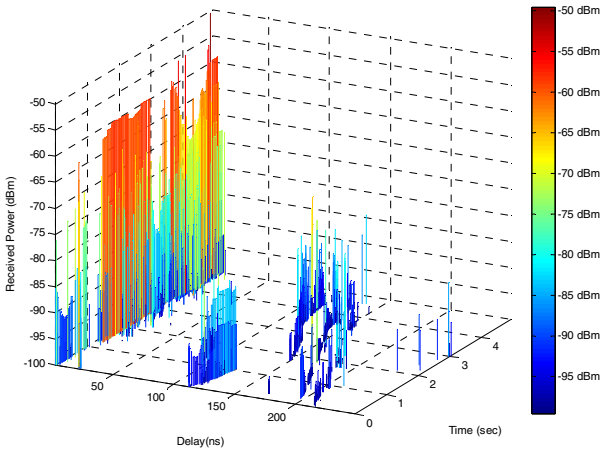

Fig. 6 PDPs for link from soldier B to soldier A for the duration of stage 1 [Fig 5, 4].

Compared to Fig. 7, Fig. 8 shows the channel impulse characteristics in which both ends of the link are typically moving within an indoor environment. It can be seen that the number of main signal components and associated ray clusters has vastly increased. The maximum rms delay spread for stage 3 was 160 ns [Table 1, 4], which, as Fig. 9 indicates, is a relatively rare event. The similar shapes of the rms delay spread CDFs in Fig. 9 also suggest that a single wideband equalizer may be used for all wireless channels in this scenario. This trend was also repeated for stages 1 and 2; this in turn means that the complexity of mm-wave transceivers for soldier-centric communications design is reduced.

V. Conclusions

This work has demonstrated the effective use of animation software combined with a commercial ray launching engine to perform channel predictions for dynamic human body movements in complex environments. Simulations of mm-wave body-to-body signal propagation were performed and the results have shown that rms angle spread was greatest within indoor environments, while the most significant delay dispersion was found outdoors and in large building structures.

Acknowledgment

This work was supported by the U.K. Ministry of Defence through the "Competition of Ideas" Program under project reference RT/COM/5/001.

References

[1] G. Felic & E. Skafidas, "Flip-Chip Interconnection Effects on 60 GHz Microstrip Antenna Performance," *IEEE Antennas and Wireless Propagation Letters*, May 2009, vol 8, pp. 283–286.

[2] S. K. Reynolds *et al.*, "A Silicon 60 GHz Receiver and Transmitter Chipset for Broadband Communications," *IEEE J. Solid-State Circuits*, vol. 41, no. 12, Dec. 2006, pp. 2820–31.

[3] K. Kunz & R. Luebbers, *The Finite Difference Time Domain Method for Electromagnetics*, CRC Press, Boca Raton FL, 1993.

[4] S. L. Cotton, W. G. Scanlon & B. K. Madahar, "Millimeter-wave soldier-to-soldier communications for covert battlefield operations," *IEEE Communications Magazine*, *Special Issue on Military Comms.*, vol. 47, 10, pp. 72–81, Oct. 2009.

[5] http://www.actix.com/radioplan_rps/

[6] J. C. Liberti and T. S. Rappaport, *Smart Antennas for Wireless Communications: IS-95 and Third Generation CDMA Applications*, Prentice Hall PTR, 1999.

[7] http://www.ist-broadway.org/documents/deliverables/broadway-wp3-d7R3_annex1.pdf

[8] A. Molisch, *Wireless Communications*, IEEE Press, Wiley, 2005.

[9] K. Witrisal, "On Estimating the rms Delay Spread from the Frequency-Domain Level Crossing Rate," *IEEE Communications Letters*, vol. 5, no. 7, pp. 287–289, Jul. 2001.

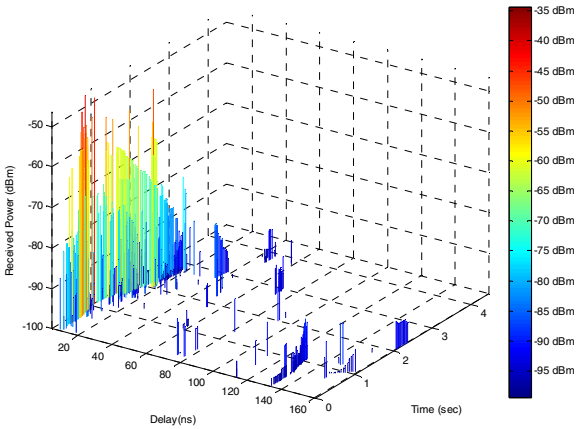

Fig. 7 PDPs for link from soldier B to soldier A for the duration of stage 2.

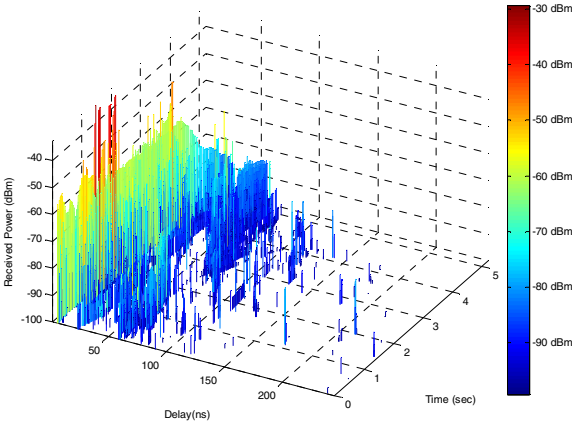

Fig. 8 PDPs for link from soldier B to soldier A for the duration of stage 3.

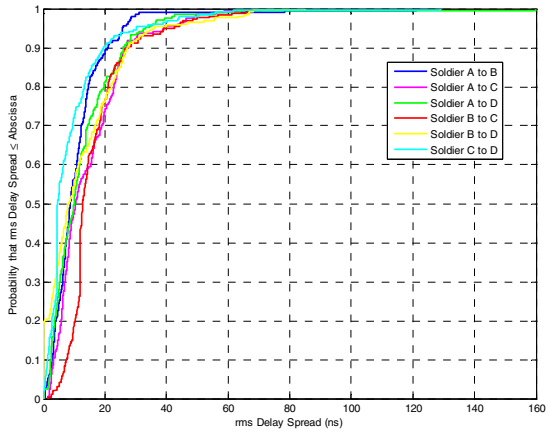

Fig. 9 CDFs of all rms delay spreads calculated for each bidirectional link over the duration of stage 3 [Fig 6, 4].

TABLE I
Summary Statistics for rms Delay Spread for all Bidirectional Soldier-to-Soldier Links as the Squad Completed Stage 1.

Link	Median rms Delay Spread (ns)	IQR rms Delay Spread (ns)	Max rms Delay Spread (ns)	Min rms Delay Spread (ns)
A to B	11.15	25.69	116.84	1.41
A to C	8.75	25.16	106.35	0.01
A to D	11.88	18.23	85.25	0.14
B to C	6.02	13.34	162.54	1.45
B to D	10.16	20.19	84.95	0.34
C to D	6.72	9.75	99.04	0.80

TABLE II
Summary Statistics for rms Delay Spread for all Bidirectional Soldier-to-Soldier Links as the Squad Completed Stage 2.

Link	Median rms Delay Spread (ns)	IQR rms Delay Spread (ns)	Max rms Delay Spread (ns)	Min rms Delay Spread (ns)
A to B	8.94	13.50	66.09	0.21
A to C	3.53	3.83	21.63	0.11
A to D	4.66	5.82	30.03	~0.00
B to C	5.66	6.47	96.11	0.59
B to D	7.23	8.95	90.52	~0.00
C to D	5.66	5.42	35.15	0.13